Large-Area Atomically Thin MoS_2 Nanosheets Prepared Using Electrochemical Exfoliation

Na Liu,[†] Paul Kim,[†] Ji Heon Kim,[†] Jun Ho Ye,[†] Sunkook Kim,[‡] and Cheol Jin Lee[†,*]

[†]School of Electrical Engineering, Korea University, Seoul 136-713, Republic of Korea, and [‡]Department of Electronics and Radio Engineering, Kyung Hee University, Yongin, Gyeonggi 446-701, Republic of Korea

ABSTRACT Molybdenum disulfide (MoS_2) is an extremely intriguing material because of its unique electrical and optical properties. The preparation of large-area and high-quality MoS_2 nanosheets is an important step in a wide range of applications. This study demonstrates that monolayer and few-layer MoS_2 nanosheets can be obtained from electrochemical exfoliation of bulk MoS_2 crystals. The lateral size of the exfoliated MoS_2 nanosheets is in the 5−50 μm range, which is much larger than that of chemically or liquid-phase exfoliated MoS_2 nanosheets. The MoS_2 nanosheets undergo low levels of oxidation during electrochemical exfoliation. In addition, microscopic and spectroscopic characterizations indicate that the exfoliated MoS_2 nanosheets are of high quality and have an intrinsic structure. A back-gate field-effect transistor was fabricated using an exfoliated monolayer MoS_2 nanosheet. The on/off current ratio is over 10^6, and the field-effect mobility is approximately 1.2 $cm^2 V^{-1} s^{-1}$; these values are comparable to the results for micromechanically exfoliated MoS_2 nanosheets. The electrochemical exfoliation method is simple and scalable, and it can be applied to exfoliate other transition metal dichalcogenides.

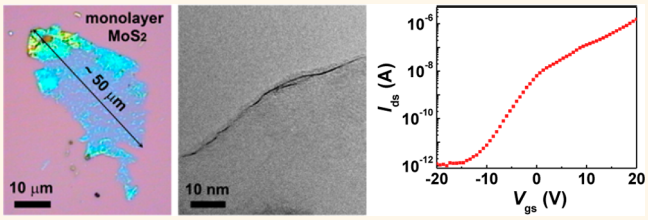

KEYWORDS: electrochemical exfoliation · MoS_2 nanosheets · field-effect transistor · layered material · solution process

Two-dimensional (2D) materials have attracted great attention in the past decade.[1−3] Graphene is by far the best-known 2D material because of its outstanding physical,[4] optical,[5] and mechanical properties,[6] although its zero band gap limits its application in low-power electronics and digital circuits.[7] Recently, considerable interest has focused on transition metal dichalcogenides, especially molybdenum disulfide (MoS_2), because they are atomically thin and possess a large band gap.[8] Structurally analogous to graphene, layered MoS_2 comprises planes wherein the S−Mo−S atoms are covalently bonded and the neighboring planes attach to each other through van der Waals forces. Like graphite, bulk MoS_2 crystals can be easily exfoliated along these planes because of the weak interlayer interactions.[9]

MoS_2 exhibits unique properties and has great potential in electronic, optoelectronic, and energy-harvesting applications.[10−16] The electronic properties of MoS_2 are strongly dependent on the number of layers.[17] Multilayer MoS_2 is an indirect-band gap semiconductor, with a gap of around 1.2 eV.[18] On the other hand, when the number of layers decreases to one, the monolayer MoS_2 turns into a direct-band gap semiconductor with a gap of around 1.8 eV.[19] Monolayer MoS_2 field-effect transistors (FETs) with a hafnium-oxide gate dielectric demonstrated typical mobilities that are over 200 $cm^2 V^{-1} s^{-1}$ and on/off current ratios as high as 10^8 at room temperature.[10] Monolayer MoS_2 is suitable for applications in flexible transistors and sensors, which is because it possesses mechanical strength 30 times higher than that of steel.[20−22] A great enhancement of photoluminescence (PL) has been detected in monolayer MoS_2, and it is related to quantum-confinement effects resulting from the indirect-to-direct band gap transition.[19,23] In one study, a photodetector fabricated using monolayer MoS_2 showed an ultrahigh photoresponsivity of 880 A W^{-1}, which is 10^5 times better than that of a graphene photodetector (6.1 mA W^{-1}).[13,24] In addition,

* Address correspondence to cjlee@korea.ac.kr.

Received for review March 24, 2014 and accepted June 17, 2014.

Published online June 17, 2014
10.1021/nn5016242

MoS_2 and its nanocomposites are considered attractive electrode materials for applications in Li-ion batteries because of their excellent charge-storage capacity and cycling performance.[14,25,26]

Large-area, atomically thin MoS_2 nanosheets must be prepared for such applications. Micromechanically exfoliated MoS_2 nanosheets with high-quality and high crystallinity have been used in fundamental studies.[10,13,19,23,27,28] However, this method is very inefficient, and the experimental results are not repeatable because of the random thickness and size of the exfoliated MoS_2 nanosheets. Thin-layer MoS_2 has been synthesized using chemical vapor deposition.[29,30] However, it is still difficult to resolve issues concerning large-scale and layer-controlled growth. A solution-processing approach is required to produce large amounts of MoS_2 nanosheets.

It has been known for many years that Li intercalation can exfoliate layered compounds, such as MoS_2, into monolayers.[31,32] Because of structural deformation, however, this chemical exfoliation method results in the loss of the MoS_2 nanosheets' semiconducting properties.[33] In addition, it is difficult to remove the residual Li which produces a doping effect in the MoS_2 nanosheets. Other shortcomings of this method include the large amount of time required and extreme sensitivity to ambient conditions. The lateral size of the chemically exfoliated MoS_2 nanosheets is typically smaller than 1 μm. Many recent studies have reported on liquid-phase exfoliation of bulk MoS_2 powder in various organic solvents or aqueous surfactant solutions with assisted sonication.[34−36] This method produces the massive quantities of MoS_2 nanosheets necessary for fabricating films and composites. However, most of the exfoliated MoS_2 nanosheets exist as multilayers, and very few are monolayered. Furthermore, their lateral size is relatively small, typically in the range of 200−500 nm. Recently, an electrochemical route has been applied to produce thin MoS_2 nanosheets, but more detailed and in-depth studies are needed.[37] Hence, the development of a feasible technique is critical to obtaining high-quality thin MoS_2 nanosheets with large areas.

In this study, we demonstrate that atomically thin MoS_2 nanosheets can be prepared by electrochemical exfoliation of the bulk MoS_2 crystal. The exfoliated MoS_2 nanosheets have lateral sizes that are as large as 50 μm. In addition, they exhibit a low degree of oxidation, high quality, and an intrinsic structure. A back-gate FET fabricated on exfoliated monolayer MoS_2 exhibits a high on/off current ratio and good field-effect mobility. The excellent properties of the MoS_2 nanosheets obtained by this method are comparable to those of mechanically exfoliated MoS_2 nanosheets.

RESULTS AND DISCUSSION

Figure 1a shows a schematic illustration of the experimental setup for the electrochemical exfoliation of bulk MoS_2 crystals. A bulk MoS_2 crystal, a Pt wire, and a 0.5 M Na_2SO_4 solution were used as a working electrode, a counter electrode, and an electrolyte, respectively. A DC bias was applied between MoS_2 and the Pt wire for the electrochemical exfoliation. A low positive bias of +2 V was initially applied to the working electrode for 10 min to wet the bulk MoS_2 crystal. The bias was then increased to +10 V for 0.5−2 h to exfoliate the crystal. As a result, many MoS_2 flakes dissociated from the bulk crystal and became suspended in the solution (Figure 1b and c). A summary of the electrolytes and exfoliation conditions tested in this work, together with the key results are listed in Table S1 (Supporting Information). The exfoliated MoS_2 flakes were collected using vacuum filtration and then redispersed in *N*-methyl-2-pyrrolidone (NMP) to obtain a uniformly distributed MoS_2-nanosheet solution (Figure 1d).[34] The concentration of obtained MoS_2-nanosheet dispersions has a range of 0.007−0.014 mg mL^{-1} and the yield of MoS_2 nanosheets is about 5−9% (Figure S1, Supporting Information).

The mechanism of electrochemical exfoliation of bulk MoS_2 crystals is described in Figure 1e. First, by applying a positive bias to the working electrode, the oxidation of water produces •OH and •O radicals assembled around the bulk MoS_2 crystal. The •OH and •O radicals and/or SO_4^{2-} anions insert themselves between the MoS_2 layers and weaken the van der Waals interactions between the layers. Second, oxidation of the radicals and/or anions leads to a release of O_2 and/or SO_2, which causes the MoS_2 interlayers to greatly expand.[38] Finally, MoS_2 flakes are detached from the bulk MoS_2 crystal by the erupting gas and are then suspended in the solution. The surface of the bulk MoS_2 crystal should be oxidized during electrochemical exfoliation, and this is directly related to the quality and degree of oxidation of the exfoliated MoS_2 nanosheets. By optimizing the experimental conditions, we obtained a bulk MoS_2 crystal with a barely oxidized surface (see Experimental Section and Figure S2, Supporting Information).

Figure 2a shows a transmission electron microscopy (TEM) image of a thin MoS_2 nanosheet with a lateral size of about 10 μm. The high-resolution TEM (HRTEM) image in Figure 2b shows a folded edge of a monolayer MoS_2 nanosheet. Figure 2c reveals that the hexagonal lattice structure of the MoS_2 nanosheet was not damaged during the electrochemical exfoliation process. The white blur on the surface of the MoS_2 nanosheet is probably residues.[33] The electron diffraction pattern collected from the exfoliated MoS_2 nanosheets in Figure 2d shows the hexagonal symmetry characteristic of 2H-MoS_2.[39] The HRTEM results indicate that the thin MoS_2 nanosheets obtained in this study exhibit few defects, high crystallinity, and an intrinsic structure.

Figure 3a shows an optical microscope image of a typical electrochemically exfoliated MoS_2 nanosheet

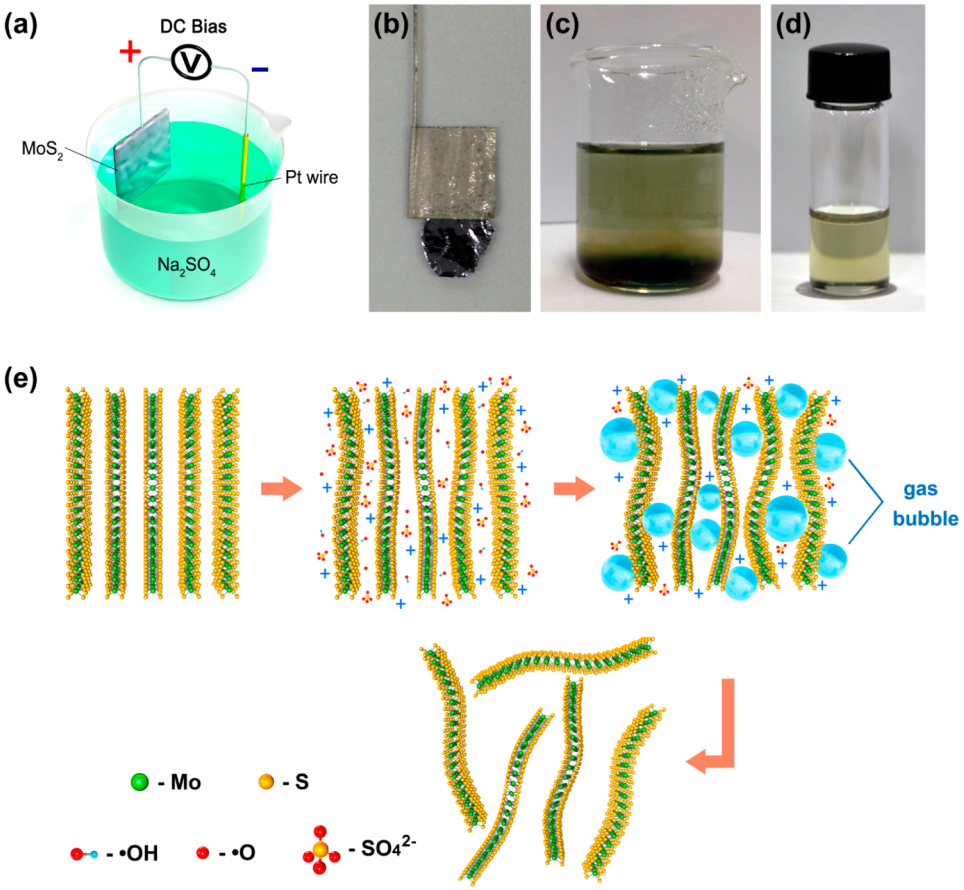

Figure 1. (a) Schematic illustration of experimental setup for electrochemical exfoliation of bulk MoS_2 crystal. (b) Photograph of a bulk MoS_2 crystal held by a Pt clamp before exfoliation. (c) Exfoliated MoS_2 flakes suspended in Na_2SO_4 solution. (d) MoS_2 nanosheets dispersed in NMP solution. (e) Schematic illustration for mechanism of electrochemical exfoliation of bulk MoS_2 crystal.

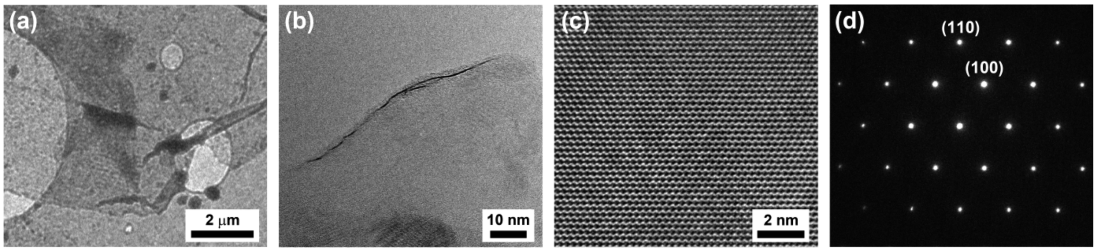

Figure 2. (a) TEM image of a thin MoS_2 nanosheet. (b) HRTEM image of a monolayer MoS_2 nanosheet showing layer edge. (c) HRTEM image of hexagonal lattice structure of a MoS_2 nanosheet. (d) Diffraction pattern of an exfoliated MoS_2 nanosheet.

deposited on a SiO_2/Si substrate by dip coating. The lateral size of the MoS_2 nanosheet is about 25 μm. More optical microscope images of the exfoliated MoS_2 nanosheets are shown in Figure S3a (Supporting Information). The electrochemically exfoliated nanosheets exhibit lateral sizes in the range of 5−50 μm, which is much larger than that of chemically and liquid-phase exfoliated MoS_2 nanosheets.[32−36] On the basis of their optical contrasts, we found that the exfoliated MoS_2 nanosheets had different number of layers in one sheet,[40] which is attributed to non-uniform distribution of surface resistance inducing the current damage.

The Raman frequencies of in-plane E^1_{2g} and out-of-plane A_{1g} modes can be used as reliable and convenient features to identify the number of layers in atomically thin MoS_2 nanosheets.[28,41] The obtained monolayer and few-layer MoS_2 nanosheets were characterized using Raman spectroscopy (Figure S4a, Supporting Information). The 514.5 nm laser line was excited using a power of <1 mW to avoid any heating effects. All of the spectra show two peaks around 384 (E^1_{2g} mode) and 407 cm^{-1} (A_{1g} mode); the two modes exhibit a well-defined dependence on the number of layers. The frequency of the E^1_{2g} mode decreases while that of the A_{1g} mode increases with increasing number

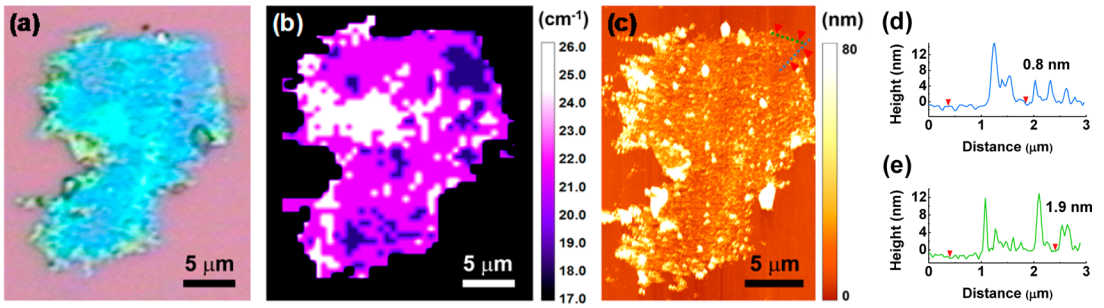

Figure 3. (a) Optical microscope image, (b) spatial map of the difference between Raman frequency of the E^1_{2g} and A_{1g} modes (excitation laser: 523 nm), and (c) AFM topography of an electrochemically exfoliated MoS_2 nanosheet on SiO_2 substrate. (d,e) Height profiles along the blue and green dash lines in (c), indicating the thickness of a monolayer and a bilayer, respectively.

of layers. These results are consistent with mechanically exfoliated MoS_2, which indicates that the obtained MoS_2 nanosheets are of high quality.

To better understand the uniformity of the layer thickness, we constructed a spatial map depicting the difference between the Raman frequencies of the E^1_{2g} and A_{1g} modes of the MoS_2 nanosheet presented in Figure 3b. The map reveals that the majority of the MoS_2 nanosheet is bilayer (pink region), but parts of it are monolayer (purple region) and in bulk form (white region). This result is consistent with the optical microscope image. Atomic force microscopy (AFM) was used to evaluate the topographies of the exfoliated MoS_2 nanosheets (Figures 3c and S5, Supporting Information). We can clearly see folds and aggregations in the AFM images, which were generated during the deposition and drying processes, and these features lead to exfoliated MoS_2 nanosheets with rough surfaces.[34] In Figure 3d and e, the height profiles show that the thickness of the monolayer and bilayer MoS_2 is about 0.8 and 1.9 nm, respectively. Our results agree with the typical thickness of monolayer MoS_2 exfoliated in a solution process which is about 0.9−1.3 nm.[32,33,42] To understand the distribution of the thickness, 100 MoS_2 nanosheets deposited on SiO_2/Si substrate were randomly selected. About 7% of these MoS_2 nanosheets are monolayer and more than 70% of them comprised 2−5 layers (Figure S6, Supporting Information).

In addition to Raman characteristics, we also investigated the PL properties of the exfoliated MoS_2 nanosheets. The PL spectra were investigated using 514.5 nm laser excitation at room temperature and normalized using the intensity of A_{1g} Raman peaks for direct comparison. Figure 4a shows the PL spectra of a monolayer MoS_2 nanosheet before and after thermal annealing. The PL spectrum of the as-prepared monolayer MoS_2 nanosheet contains two peaks located at 669 and 622 nm, which correspond to the A1 and B1 direct excitonic transitions at 1.85 and 1.99 eV, respectively.[23] For the nanosheet that was annealed at 200 °C in a N_2 environment for 2 h, the PL intensity is higher by a factor of 10. This is because the residual solvent absorbed by the MoS_2 nanosheet surface

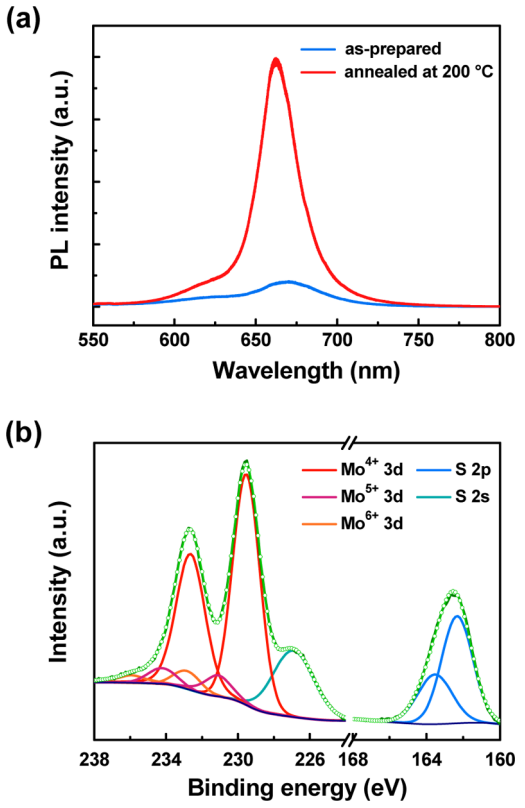

Figure 4. (a) PL spectra of monolayer MoS_2 before and after thermal annealing at 200 °C in N_2 for 2 h (excitation laser: 514.5 nm; data were normalized using the intensity of A_{1g} Raman peaks). (b) XPS characterization of an as-prepared MoS_2 nanosheet.

evaporated. We also investigated the PL spectra of exfoliated MoS_2 nanosheets with different numbers of layers (Figure S4b, Supporting Information). The strongest PL signal appears in the spectrum for monolayer MoS_2, while the emission intensity significantly decreases as the number of layers increases. The different PL properties of the monolayer and few-layer MoS_2 nanosheets agree with the fact that monolayer MoS_2 has a direct band gap structure and few-layer MoS_2 has an indirect one.[19,23]

The surface chemical properties of an as-prepared MoS_2 nanosheet were studied using X-ray photoelectron spectroscopy (XPS) (Figure 4b). The Mo 3d spectrum shows two strong peaks at 229.5 and 232.6 eV

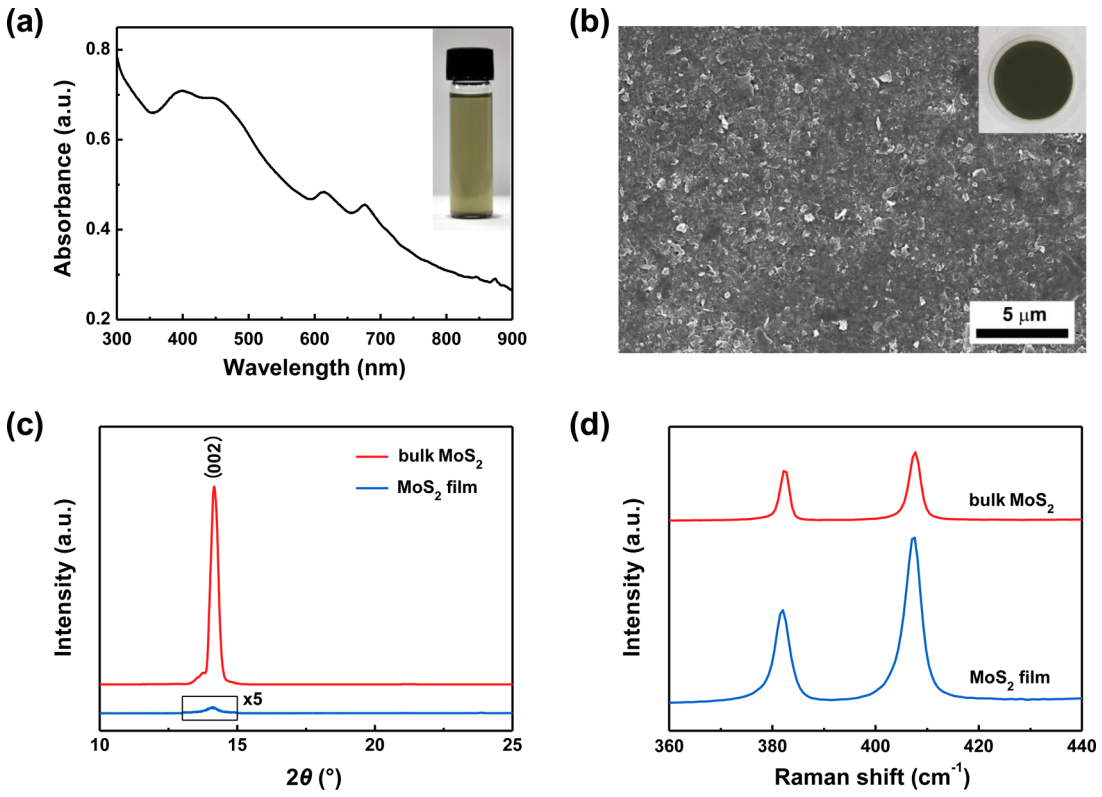

Figure 5. (a) UV−visible absorption spectrum of MoS_2 nanosheets dispersed in NMP solution. Inset: Photograph of MoS_2 nanosheet dispersed in NMP (0.011 mg mL^{-1}). (b) SEM image of surface of MoS_2 thin film. Inset: Photograph of MoS_2 thin film on an aluminum oxide membrane (25 mm in diameter). (c) XRD patterns and (d) Raman spectra of MoS_2 thin film and bulk MoS_2 crystal.

corresponding to Mo^{4+} $3d_{5/2}$ and Mo^{4+} $3d_{3/2}$, respectively.[32,43] Additionally, the spectrum shows four weak peaks at 231.1 and 234.2 eV corresponding to Mo^{5+} $3d_{5/2}$ and Mo^{5+} $3d_{3/2}$, respectively; at 232.8 and 235.9 eV corresponding to Mo^{6+} $3d_{5/2}$ and Mo^{6+} $3d_{3/2}$, respectively.[44] In the S 2p spectrum, two peaks are observed at 162.3 and 163.5 eV corresponding to S $2p_{3/2}$ and S $2p_{1/2}$, respectively. These results are consistent with the reported values for MoS_2 single crystals, indicating that the obtained MoS_2 nanosheets are the 2H phase.[33] This is in contrast to the chemically exfoliated MoS_2 nanosheets that lose their pristine semiconducting properties because their structure changes from 2H to 1T phase as a result of Li intercalation. The Mo^{5+} and Mo^{6+} are thought to be generated by the oxidation of MoS_2 during electrochemical exfoliation; the total amount of them is approximately 15.6 at. %, which indicates that the exfoliated MoS_2 nanosheets have a low degree of oxidation. The Mo^{6+} can be reduced to Mo^{5+} by thermal annealing in N_2 (Figure S7 and Table S2, Supporting Information).[45]

A dispersion of MoS_2 nanosheets in NMP with a concentration of about 0.011 mg mL^{-1} was characterized using UV−visible absorption spectroscopy (Figure 5a). The spectrum shows two excitonic peaks at 676 nm (1.83 eV) and 613 nm (2.02 eV), which are related to A1 and B1 *via* direct transition with energy separation, suggesting the existence of high-quality semiconducting MoS_2 nanosheets.[33,46] A MoS_2 thin film can be fabricated using the solution by applying vacuum filtration. Figure 5b shows the scanning electron microscopy (SEM) image of the surface of a MoS_2 thin film. It can be seen that the large MoS_2 nanosheets form a smooth plane and many small flakes reside on it.

We analyzed the X-ray diffraction (XRD) (Figure 5c) and Raman spectroscopy (Figure 5d) results of the MoS_2 thin film. An initial bulk MoS_2 crystal before electrochemical exfoliation was also measured for comparisons. In the XRD patterns, the (002) reflection of the MoS_2 thin film is significantly smaller than that of the bulk MoS_2 crystal, which indicates that a large number of the MoS_2 nanosheets prepared were highly exfoliated.[47] The Raman spectra of both the thin film and bulk crystal of MoS_2 show two peaks at 382 and 407 cm^{-1}. The intense Raman peaks of the MoS_2 thin film offer strong evidence that the exfoliated MoS_2 nanosheets are of high quality.

To evaluate the electrical properties of the exfoliated MoS_2 nanosheets, back-gate FETs were fabricated by depositing Au/Ti electrodes *via* electron-beam evaporation onto the top of the MoS_2 nanosheets on SiO_2/Si substrates. Figure 6a and b show, respectively, an optical microscope image of a monolayer MoS_2 nanosheet and an SEM image of a transistor device

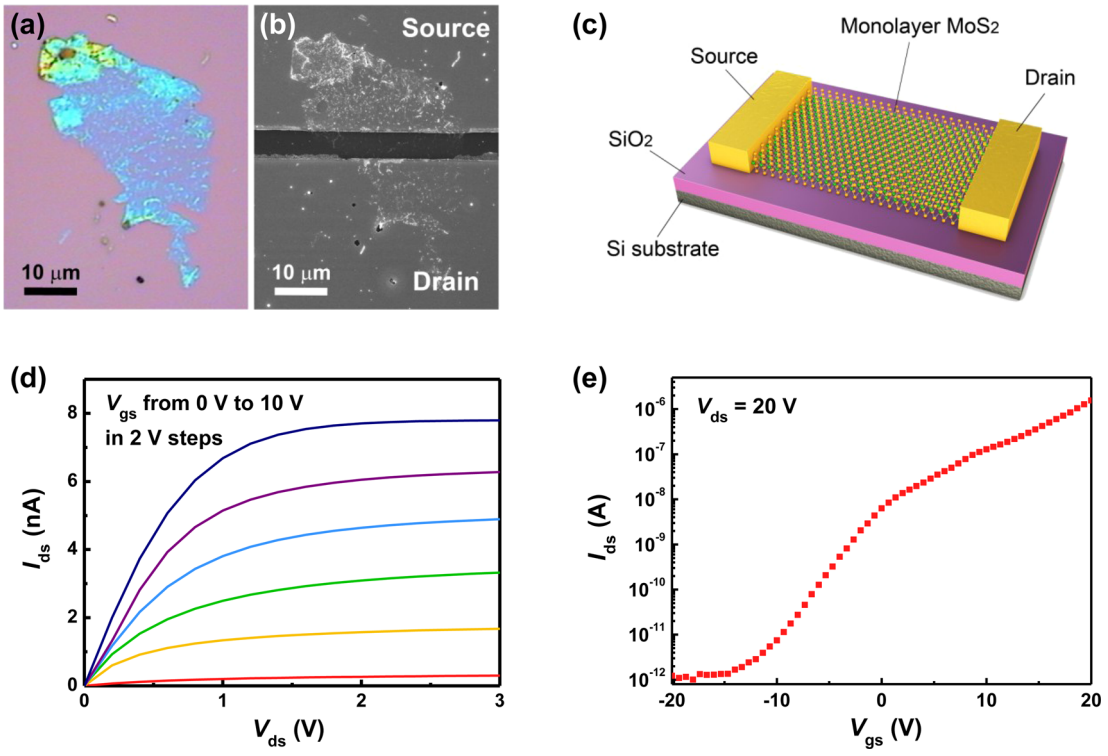

Figure 6. (a) Optical microscope image of an electrochemically exfoliated monolayer MoS_2 nanosheet deposited on SiO_2 substrate. (b) SEM image of a back-gate transistor based on the electrochemically exfoliated monolayer MoS_2 in (a). (c) 3D schematic of a monolayer MoS_2 transistor. (d) Output characteristics at different V_{gs} values for the monolayer MoS_2 transistor. (e) Transfer characteristics at V_{ds} = 20 V on a log scale. The on/off current ratio is above 10^6 and the field-effect mobility is approximately 1.2 $cm^2\ V^{-1}\ s^{-1}$.

fabricated on it. The lateral size of the monolayer MoS_2 nanosheet is as large as 50 μm. The channel region of the MoS_2 FET was measured using AFM and the Raman spatial map to determine the thickness and uniformity of the MoS_2 nanosheet (Figure S8, Supporting Information). The height profile shows that the thickness is approximately 0.7 nm, which is consistent with previous theoretical and experimental values.[9,10,48] Additionally, it shows that the monolayer MoS_2 is almost homogeneous, even on the 20-μm scale, with the exception of a few thick spots. A three-dimensional (3D) schematic of the monolayer MoS_2 device structure is shown in Figure 6c.

Figure 6d displays the output characteristics (drain current I_{ds} *vs* drain voltage V_{ds}) at different gate voltages (V_{gs}) for the monolayer MoS_2 transistor. The $I_{ds}-V_{ds}$ curves show linear characteristics and clear current saturation at low and high drain voltage, respectively. The transfer characteristics (drain current I_{ds} *vs* gate voltage V_{gs}) of this device are shown in Figure 6e. The field-effect mobility (μ) was estimated in the saturation regime using the following equation:

$$I_{ds} = \frac{WC_{ox}}{2L}\mu(V_{gs} - V_{th})^2$$

where L is the channel length, W is the channel width, C_{ox} is the gate capacitance, and V_{th} is the threshold voltage. For V_{ds} = 20 V, the calculated field-effect mobility of the monolayer MoS_2 transistor is around 1.2 $cm^2\ V^{-1}\ s^{-1}$, and the on/off current ratio is higher than 10^6. The small spots in Figure S8b (Supporting Information) may represent thick flakes or wrinkles in monolayer MoS_2 nanosheet.[49,50] These flakes or wrinkles would have degraded the performance of the device owing to the chemisorption of oxygen and water at the flakes' edges and the introduction of interlayer resistance.[51,52] Even so, the calculated field-effect mobility is much higher than that for the previously mentioned liquid-phase exfoliated MoS_2 nanosheets (0.01 $cm^2\ V^{-1}\ s^{-1}$),[34] and it is also comparable to previously reported data collected from mechanically exfoliated monolayer MoS_2 devices (0.1−10 $cm^2\ V^{-1}\ s^{-1}$).[10,53−55] Note that the FET shows typical n-type field-effect behavior; this is very different from the chemically exfoliated MoS_2 nanosheets that show p-type behavior as a doping effect of the residual Li.[32] Our MoS_2 nanosheets were directly detached from the bulk MoS_2 crystal through the insertion of electrolyte ions, as well as production and eruption of gases. As a result, these MoS_2 nanosheets retain their intrinsic properties and structures.

CONCLUSION

We have demonstrated that monolayer and few-layer MoS_2 nanosheets can be prepared by electrochemically exfoliating the bulk MoS_2 crystal in an ionic

solution. The lateral size of the exfoliated MoS_2 nanosheets can reach 50 μm, which is much larger than that of mechanically, chemically and liquid-phase exfoliated MoS_2 nanosheets. The n-type FET based on the exfoliated monolayer MoS_2 exhibits an on/off current ratio of over 10^6 and a field-effect mobility of around 1.2 $cm^2\ V^{-1}\ s^{-1}$. This electrical performance analysis, when combined with TEM, Raman, PL and XPS measurements, confirm that the exfoliated MoS_2 nanosheets exhibit high quality, an intrinsic structure, and a low degree of oxidation. This work provides a simple, efficient and scalable approach to preparing large-area atomically thin MoS_2 nanosheets, which are promising for a wide range of applications.

EXPERIMENTAL SECTION

Electrochemical Exfoliation of MoS_2. Natural, single-crystalline bulk MoS_2 (SPI Supplies, 429MM-AB) was used as the working electrode and source for the electrochemical exfoliation. The bulk MoS_2 crystal was clamped to a Pt clip and the MoS_2 crystal alone was immersed in the ionic solution. A grounded Pt wire was used as the counter electrode and was placed 2 cm away from, and parallel to, the bulk MoS_2 crystal. The 0.5 M Na_2SO_4 solution was prepared by mixing 4.0 g of sodium hydroxide (Duksan) and 5.2 g of sulfuric acid (95%, Samchun) dilute solutions, then adding DI water to obtain 100 mL of the combined solution.

The electrochemical exfoliation process was carried out by applying a positive bias on the working electrode. The intensity of the electrochemical reaction could be estimated by the amount of gas bubbles produced on the MoS_2 bulk surface. After the electrochemical-exfoliation efficiency was optimized, the bulk MoS_2 crystal developed a barely oxidized surface when the Pt clip was 0.5 cm above the liquid level. In the exfoliation process, electrolysis of water released O_2 and H_2, which led to a drawdown of the liquid level. This caused the current passing through two electrodes to decrease with increasing time. To eliminate the effect of current variation on experimental results, we used a tube to connect the experimental setup (shown in Figure 1a) with a big beaker that also contained the 0.5 M Na_2SO_4 solution. The beaker was big enough to allow us to ignore the lower liquid-level drawdown because of water electrolysis. As a result, the current remained stable during the exfoliation process.

The exfoliated MoS_2 flakes were collected using porous membranes (0.2 μm, JGWP, Millipore) and washed with DI water using vacuum filtration. After drying, the collected MoS_2 flakes were redispersed in an NMP solution, using low-power sonication in a water-bath for 1 h and centrifugation at 1500 rpm for 30 min to remove the unwanted thick MoS_2 flakes. The top half of the solution was used for further characterization and film fabrication.

Characterizations. The MoS_2 nanosheets prepared using electrochemical exfoliation were deposited by dip coating onto a 300 nm SiO_2/Si substrate for optical microscopy, Raman, PL, XPS, and AFM studies. Raman and PL spectra were measured using a multipurpose spectrometer (LabRAM HR800, Horiba Jobin Yvon) with laser excitation at 514.5 nm. The PL spectra were normalized using the intensity of A_{1g} Raman peaks. Raman spatial mappings were measured using a combined Raman and FTIR microscope system (LabRAM ARAMIS IR^2, Horiba Jobin Yvon) with laser excitation at 523 nm. The Raman and PL analyses were performed in ambient conditions, the power of the laser lines was below 1 mW, the laser spot-size was approximately 1 μm, and the Si peak at 520.7 cm^{-1} was used as a reference for wavenumber calibration. The XPS measurements were performed using an Ulvac PHI X-tool spectrometer with Al Kα X-ray radiation (1486.6 eV). The binding energies were calibrated with C 1s at 284.5 eV. The AFM images were obtained using a microscope (XE-100, PSIA) in noncontact mode. The atomic structure of the MoS_2 nanosheets was characterized using a TEM (Tecnai G2 F30 ST, FEI) with an accelerating voltage of 300 eV. The SEM images were taken using a field-emission SEM (FE-SEM; S-4800, Hitachi) coupled with energy-dispersive X-ray spectroscopy (EDS). Absorption spectra were collected for a MoS_2 thin film in a Varian Cary 50 UV−visible spectrophotometer. XRD patterns were recorded on an X-ray diffractometer (D/Max-2500, Rigaku) using Cu Kα radiation. The electrical measurements were carried out at room temperature in ambient conditions using a probe station (CPX-VF, Lakeshore).

Fabrication of MoS_2 Thin Films. The MoS_2 nanosheets dispersed in the NMP solution were first vacuum-filtered through a porous membrane (0.02 μm, Anodisc, Whatman or 0.2 μm, JGWP, Millipore). They were then washed with isopropyl alcohol and DI water. After that, the film was peeled off and dried in an air oven at 80 °C for 2 h to evaporate the residual moisture.

Fabrication of MoS_2 Field-Effect Transistors. The exfoliated MoS_2 nanosheets were deposited onto a 300 nm SiO_2/Si substrate using the dip-coating method. They were then dried at room temperature for 1 h. After that, the MoS_2 nanosheets were carefully washed with DI water and dried again. The Au/Ti electrical contacts on MoS_2 were fabricated using photolithography and electron-beam evaporation of Ti (10 nm) and Au (50 nm), followed by annealing at 150 °C in a vacuum oven for 2 h.

Conflict of Interest: The authors declare no competing financial interest.

Acknowledgment. The authors would like to thank Dr. Xueqiu You for his helpful comments. This work was supported by World Class University (WCU, *R*32-2008-000-10082-0) Project and by International Cooperation of Science & Technology project (KICOS, 2009-00299) through the National Research Foundation of Korea funded by the Ministry of Education, Science and Technology. It was also supported by the Korea Basic Science Institute.

Supporting Information Available: XPS, SEM, EDS, optical microscopy, Raman, PL and AFM analyses of the electrochemically exfoliated MoS_2 nanosheets. This material is available free of charge *via* the Internet at http://pubs.acs.org.

REFERENCES AND NOTES

1. Novoselov, K. S.; Geim, A. K.; Morozov, S. V.; Jiang, D.; Zhang, Y.; Dubonos, S. V.; Grigorieva, I. V.; Firsov, A. A. Electric Field Effect in Atomically Thin Carbon Films. *Science* **2004**, *306*, 666–669.
2. Huang, X.; Qi, X.; Boey, F.; Zhang, H. Graphene-Based Composites. *Chem. Soc. Rev.* **2012**, *41*, 666–686.
3. Huang, X.; Yin, Z.; Wu, S.; Qi, X.; He, Q.; Zhang, Q.; Yan, Q.; Boey, F.; Zhang, H. Graphene-Based Materials: Synthesis, Characterization, Properties, and Applications. *Small* **2011**, *7*, 1876–1902.
4. Novoselov, K. S.; Geim, A. K.; Morozov, S. V.; Jiang, D.; Katsnelson, M. I.; Grigorieva, I. V.; Dubonos, S. V.; Firsov, A. A. Two-Dimensional Gas of Massless Dirac Fermions in Graphene. *Nature* **2005**, *438*, 197–200.
5. Bonaccorso, F.; Sun, Z.; Hasan, T.; Ferrari, A. C. Graphene Photonics and Optoelectronics. *Nat. Photonics* **2010**, *4*, 611–622.
6. Lee, C.; Wei, X.; Kysar, J. W.; Hone, J. Measurement of the Elastic Properties and Intrinsic Strength of Monolayer Graphene. *Science* **2008**, *321*, 385–388.
7. Schwierz, F. Graphene Transistors: Status, Prospects, and Problems. *Proc. IEEE* **2013**, *101*, 1567–1584.
8. Schwierz, F. Nanoelectronics: Flat Transistors Get off the Ground. *Nat. Nanotechnol.* **2011**, *6*, 135–136.

9. Novoselov, K. S.; Jiang, D.; Schedin, F.; Booth, T. J.; Khotkevich, V. V.; Morozov, S. V.; Geim, A. K. Two-Dimensional Atomic Crystals. *Proc. Natl. Acad. Sci. U. S. A.* **2005**, *102*, 10451–10453.
10. Radisavljevic, B.; Radenovic, A.; Brivio, J.; Giacometti, V.; Kis, A. Single-Layer MoS_2 Transistors. *Nat. Nanotechnol.* **2011**, *6*, 147–150.
11. Kim, S.; Konar, A.; Hwang, W.-S.; Lee, J. H.; Lee, J.; Yang, J.; Jung, C.; Kim, H.; Yoo, J.-B.; Choi, J.-Y.; *et al.* High-Mobility and Low-Power Thin-Film Transistors Based on Multilayer MoS_2 Crystals. *Nat. Commun.* **2012**, *3*, 1011.
12. Choi, W.; Cho, M. Y.; Konar, A.; Lee, J. H.; Cha, G.-B.; Hong, S. C.; Kim, S.; Kim, J.; Jena, D.; Joo, J.; *et al.* High-Detectivity Multilayer MoS_2 Phototransistors with Spectral Response from Ultraviolet to Infrared. *Adv. Mater.* **2012**, *24*, 5832–5836.
13. Lopez-Sanchez, O.; Lembke, D.; Kayci, M.; Radenovic, A.; Kis, A. Ultrasensitive Photodetectors Based on Monolayer MoS_2. *Nat. Nanotechnol.* **2013**, *8*, 497–501.
14. Feng, C.; Ma, J.; Li, H.; Zeng, R.; Guo, Z.; Liu, H. Synthesis of Molybdenum Disulfide (MoS_2) for Lithium Ion Battery Applications. *Mater. Res. Bull.* **2009**, *44*, 1811–1815.
15. Huang, X.; Zeng, Z.; Zhang, H. Metal Dichalcogenide Nanosheets: Preparation, Properties and Applications. *Chem. Soc. Rev.* **2013**, *42*, 1934–1946.
16. Chhowalla, M.; Shin, H. S.; Eda, G.; Li, L.-J.; Loh, K. P.; Zhang, H. The Chemistry of Two-Dimensional Layered Transition Metal Dichalcogenide Nanosheets. *Nat. Chem.* **2013**, *5*, 263–275.
17. Kuc, A.; Zibouche, N.; Heine, T. Influence of Quantum Confinement on the Electronic Structure of the Transition Metal Sulfide TS_2. *Phys. Rev. B: Condens. Matter Mater. Phys.* **2011**, *83*, 245213.
18. Roxlo, C. B.; Chianelli, R. R.; Deckman, H. W.; Ruppert, A. F.; Wong, P. P. Bulk and Surface Optical-Absorption in Molybdenum-Disulfide. *J. Vac. Sci. Technol., A* **1987**, *5*, 555–557.
19. Mak, K. F.; Lee, C.; Hone, J.; Shan, J.; Heinz, T. F. Atomically Thin MoS_2: A Direct-Gap Semiconductor. *Phys. Rev. Lett.* **2010**, *105*, 136805.
20. Chang, H.-Y.; Yang, S.; Lee, J.; Tao, L.; Hwang, W.-S.; Jena, D.; Lu, N.; Akinwande, D. High-Performance, Highly Bendable MoS_2 Transistors with High-K Dielectrics for Flexible Low-Power Systems. *ACS Nano* **2013**, *7*, 5446–5452.
21. He, Q.; Zeng, Z.; Yin, Z.; Li, H.; Wu, S.; Huang, X.; Zhang, H. Fabrication of Flexible MoS_2 Thin-Film Transistor Arrays for Practical Gas-Sensing Applications. *Small* **2012**, *8*, 2994–2999.
22. Bertolazzi, S.; Brivio, J.; Kis, A. Stretching and Breaking of Ultrathin MoS_2. *ACS Nano* **2011**, *5*, 9703–9709.
23. Splendiani, A.; Sun, L.; Zhang, Y.; Li, T.; Kim, J.; Chim, C.-Y.; Galli, G.; Wang, F. Emerging Photoluminescence in Monolayer MoS_2. *Nano Lett.* **2010**, *10*, 1271–1275.
24. Mueller, T.; Xia, F.; Avouris, P. Graphene Photodetectors for High-Speed Optical Communications. *Nat. Photonics* **2010**, *4*, 297–301.
25. Chang, K.; Chen, W. L-Cysteine-Assisted Synthesis of Layered MoS_2/Graphene Composites with Excellent Electrochemical Performances for Lithium Ion Batteries. *ACS Nano* **2011**, *5*, 4720–4728.
26. Cao, X.; Shi, Y.; Shi, W.; Rui, X.; Yan, Q.; Kong, J.; Zhang, H. Preparation of MoS_2-Coated Three-Dimensional Graphene Networks for High-Performance Anode Material in Lithium-Ion Batteries. *Small* **2013**, *9*, 3433–3438.
27. Yin, Z.; Li, H.; Li, H.; Jiang, L.; Shi, Y.; Sun, Y.; Lu, G.; Zhang, Q.; Chen, X.; Zhang, H. Single-Layer MoS_2 Phototransistors. *ACS Nano* **2012**, *6*, 74–80.
28. Lee, C.; Yan, H.; Brus, L. E.; Heinz, T. F.; Hone, J.; Ryu, S. Anomalous Lattice Vibrations of Single- and Few-Layer MoS_2. *ACS Nano* **2010**, *4*, 2695–2700.
29. Zhan, Y.; Liu, Z.; Najmaei, S.; Ajayan, P. M.; Lou, J. Large-Area Vapor-Phase Growth and Characterization of MoS_2 Atomic Layers on a SiO_2 Substrate. *Small* **2012**, *8*, 966–971.
30. Lee, Y.-H.; Zhang, X.-Q.; Zhang, W.; Chang, M.-T.; Lin, C.-T.; Chang, K.-D.; Yu, Y.-C.; Wang, J. T.-W.; Chang, C.-S.; Li, L.-J.; *et al.* Synthesis of Large-Area MoS_2 Atomic Layers with Chemical Vapor Deposition. *Adv. Mater.* **2012**, *24*, 2320–2325.
31. Joensen, P.; Frindt, R. F.; Morrison, S. R. Single-Layer MoS_2. *Mater. Res. Bull.* **1986**, *21*, 457–461.
32. Zeng, Z.; Yin, Z.; Huang, X.; Li, H.; He, Q.; Lu, G.; Boey, F.; Zhang, H. Single-Layer Semiconducting Nanosheets: High-Yield Preparation and Device Fabrication. *Angew. Chem., Int. Ed.* **2011**, *50*, 11093–11097.
33. Eda, G.; Yamaguchi, H.; Voiry, D.; Fujita, T.; Chen, M.; Chhowalla, M. Photoluminescence from Chemically Exfoliated MoS_2. *Nano Lett.* **2011**, *11*, 5111–5116.
34. Coleman, J. N.; Lotya, M.; O'Neill, A.; Bergin, S. D.; King, P. J.; Khan, U.; Young, K.; Gaucher, A.; De, S.; Smith, R. J.; *et al.* Two-Dimensional Nanosheets Produced by Liquid Exfoliation of Layered Materials. *Science* **2011**, *331*, 568–571.
35. Smith, R. J.; King, P. J.; Lotya, M.; Wirtz, C.; Khan, U.; De, S.; O'Neill, A.; Duesberg, G. S.; Grunlan, J. C.; Moriarty, G.; *et al.* Large-Scale Exfoliation of Inorganic Layered Compounds in Aqueous Surfactant Solutions. *Adv. Mater.* **2011**, *23*, 3944–3948.
36. O'Neill, A.; Khan, U.; Coleman, J. N. Preparation of High Concentration Dispersions of Exfoliated MoS_2 with Increased Flake Size. *Chem. Mater.* **2012**, *24*, 2414–2421.
37. You, X.; Liu, N.; Lee, C. J.; Pak, J. J. An Electrochemical Route to MoS_2 Nanosheets for Device Applications. *Mater. Lett.* **2014**, *121*, 31–35.
38. Lu, J.; Yang, J.; Wang, J.; Lim, A.; Wang, S.; Loh, K. P. One-Pot Synthesis of Fluorescent Carbon Nanoribbons, Nanoparticles, and Graphene by the Exfoliation of Graphite in Ionic Liquids. *ACS Nano* **2009**, *3*, 2367–2375.
39. Wypych, F.; Solenthaler, C.; Prins, R.; Weber, T. Electron Diffraction Study of Intercalation Compounds Derived from 1T-MoS_2. *J. Solid State Chem.* **1999**, *144*, 430–436.
40. Li, H.; Lu, G.; Yin, Z.; He, Q.; Li, H.; Zhang, Q.; Zhang, H. Optical Identification of Single- and Few-Layer MoS_2 Sheets. *Small* **2012**, *8*, 682–686.
41. Li, H.; Zhang, Q.; Yap, C. C. R.; Tay, B. K.; Edwin, T. H. T.; Olivier, A.; Baillargeat, D. From Bulk to Monolayer MoS_2: Evolution of Raman Scattering. *Adv. Funct. Mater.* **2012**, *22*, 1385–1390.
42. Li, H.; Qi, X.; Wu, J.; Zeng, Z.; Wei, J.; Zhang, H. Investigation of MoS_2 and Graphene Nanosheets by Magnetic Force Microscopy. *ACS Nano* **2013**, *7*, 2842–2849.
43. Brown, N. M. D.; Cui, N.; McKinley, A. An XPS Study of the Surface Modification of Natural MoS_2 Following Treatment in an RF-Oxygen Plasma. *Appl. Surf. Sci.* **1998**, *134*, 11–21.
44. Bianchi, C. L.; Cattania, M. G.; Villa, P. XPS Characterization of Ni and Mo Oxides Before and After "*In Situ*" Treatments. *Appl. Surf. Sci.* **1993**, *70*, 211–216.
45. Spevack, P. A.; McIntyre, N. S. Thermal Reduction of MoO_3. *J. Phys. Chem.* **1992**, *96*, 9029–9035.
46. Wilcoxon, J. P.; Newcomer, P. P.; Samara, G. A. Synthesis and Optical Properties of MoS_2 and Isomorphous Nanoclusters in the Quantum Confinement Regime. *J. Appl. Phys.* **1997**, *81*, 7934–7944.
47. Liang, Y.; Feng, R.; Yang, S.; Ma, H.; Liang, J.; Chen, J. Rechargeable Mg Batteries with Graphene-like MoS_2 Cathode and Ultrasmall Mg Nanoparticle Anode. *Adv. Mater.* **2011**, *23*, 640–643.
48. Wilson, J. A.; Yoffe, A. D. The Transition Metal Dichalcogenides Discussion and Interpretation of Observed Optical, Electrical and Structural Properties. *Adv. Phys.* **1969**, *18*, 193–335.
49. Castellanos-Gomez, A.; Roldán, R.; Cappelluti, E.; Buscema, M.; Guinea, F.; van der Zant, H. S.; Steele, G. A. Local Strain Engineering in Atomically Thin MoS_2. *Nano Lett.* **2013**, *13*, 5361–5366.
50. Castellanos-Gomez, A.; van der Zant, H. S.; Steele, G. A. Folded MoS_2 Layers with Reduced Interlayer Coupling. *Nano Res.* **2014**, *7*, 1–7.
51. Qiu, H.; Pan, L.; Yao, Z.; Li, J.; Shi, Y.; Wang, X. Electrical Characterization of Back-Gated Bi-Layer MoS_2 Field-Effect Transistors and the Effect of Ambient on Their Performances. *Appl. Phys. Lett.* **2012**, *100*, 123104.

52. Das, S.; Appenzeller, J. Where Does the Current Flow in Two-Dimensional Layered Systems? *Nano Lett.* **2013**, *13*, 3396–3402.
53. Lee, K.; Kim, H.-Y.; Lotya, M.; Coleman, J. N.; Kim, G.-T.; Duesberg, G. S. Electrical Characteristics of Molybdenum Disulfide Flakes Produced by Liquid Exfoliation. *Adv. Mater.* **2011**, *23*, 4178–4182.
54. Late, D. J.; Liu, B.; Matte, H. S. S. R.; Dravid, V. P.; Rao, C. N. R. Hysteresis in Single-Layer MoS_2 Field Effect Transistors. *ACS Nano* **2012**, *6*, 5635–5641.
55. Li, H.; Yin, Z.; He, Q.; Li, H.; Huang, X.; Lu, G.; Fam, D. W. H.; Tok, A. I. Y.; Zhang, Q.; Zhang, H. Fabrication of Single- and Multilayer MoS_2 Film-Based Field-Effect Transistors for Sensing NO at Room Temperature. *Small* **2012**, *8*, 63–67.